ORIGINAL ARTICLE

Lenvatinib- and vadimezan-loaded synthetic high-density lipoprotein for combinational immunochemotherapy of metastatic triple-negative breast cancer

Chao Zheng[a,b], Wen Zhang[a,b], Jinming Wang[d], Yihui Zhai[b,e], Fengqin Xiong[a,b], Ying Cai[b,e], Xiang Gong[a,b], Binyu Zhu[b,e], Helen He Zhu[d], Hao Wang[a,*], Yaping Li[b,e,f,*], Pengcheng Zhang[b,c,e,*]

[a]China State Institute of Pharmaceutical Industry, Shanghai 201203, China
[b]State Key Laboratory of Drug Research & Center of Pharmaceutics, Shanghai Institute of Materia Medica, Chinese Academy of Sciences, Shanghai 201203, China
[c]Yantai Key Laboratory of Nanomedicine & Advanced Preparations, Yantai Institute of Materia Medica, Yantai 264000, China
[d]State Key Laboratory of Oncogenes and Related Genes, Renji-Med-X Stem Cell Research Center, Department of Urology, Ren Ji Hospital, School of Medicine and School of Biomedical Engineering, Shanghai Jiao Tong University, Shanghai 200135, China
[e]University of Chinese Academy of Sciences, Beijing 100049, China
[f]Bohai Rim Advanced Research Institute for Drug Discovery, Yantai 264000, China

Abstract Metastatic triple-negative breast cancer (TNBC) is the most aggressive type of breast cancer. Combination of systemic chemotherapy and immune checkpoint blockade is effective but of limited benefit due to insufficient intratumoral infiltration of cytotoxic T lymphocytes (CTLs) and the accumulation of immunosuppressive cells. Herein, we designed a lenvatinib- and vadimezan-loaded synthetic high-density lipoprotein (LV-sHDL) for combinational immunochemotherapy of metastatic TNBC. The LV-sHDL targeted scavenger receptor class B type 1-overexpressing 4T1 cells in the tumor after intravenous injection. The multitargeted tyrosine kinase inhibitor (TKI) lenvatinib induced immunogenic cell

Lenvatinib;
Vadimezan;
Immune checkpoint
blockade

death of the cancer cells, and the stimulator of interferon genes (STING) agonist vadimezan triggered local inflammation to facilitate dendritic cell maturation and antitumor macrophage differentiation, which synergistically improved the intratumoral infiltration of total and active CTLs by 33- and 13-fold, respectively. LV-sHDL inhibited the growth of orthotopic 4T1 tumors, reduced pulmonary metastasis, and prolonged the survival of animals. The efficacy could be further improved when LV-sHDL was used in combination with antibody against programmed cell death ligand 1. This study highlights the combination use of multitargeted TKI and STING agonist a promising treatment for metastatic TNBC.

1. Introduction

Triple-negative breast cancer (TNBC) is the most aggressive type of breast cancer with the absence of receptors for estrogen, progesterone, and human epidermal growth factor 2[1,2]. The median overall survival for patients with metastatic TNBC is approximately 1 year *vs.* approximately 5 years for those with other types of breast cancer[1]. Due to its invasiveness, systemic chemotherapy after surgical tumor resection and localized radiotherapy is necessary but is limited by its short time to tumor progression and side effects[3]. Recently, increasing evidences indicate that the efficacy of chemotherapy is partially associated with its immunological effects[4,5]. Indeed, combination of nab-paclitaxel (Abraxane®) and anti-programmed cell death ligand 1 (PDL1) antibody (Atezolizumab) has been proved effective on TNBC patients[6], taking advantage of relatively higher mutation burden and lymphocyte infiltration in TNBC tumors than other types of breast cancer[7–9]. However, due to the intratumoral heterogeneity and immune-suppressive microenvironment of TNBC tumors[8–11], the efficacy of current chemotherapy alone or in combination with immunotherapy such as immune checkpoint blockade (ICB) is limited. Combination use of immunogenic cell death (ICD) inducer and immunosuppressive reversal has been recently explored to potentiate ICB with encouraging achievements[12]. Nevertheless, cytotoxic drugs are usually used, and many of them may also inhibit effector cells while killing cancer cells[5]. In addition, prescription of immunosuppressive drugs may be necessary to alleviate the side effects. A new strategy that can simultaneously improve cancer cell eradication and lymphocyte infiltration with good tolerability is of urgent need.

Targeted anticancer agents target dysregulated pathways in the cancer cells and are thus better tolerated than cytotoxic agents. For instance, lenvatinib (LEN) is a multitargeted tyrosine kinase inhibitor (TKI) blocking receptors such as vascular endothelial growth factor receptors (VEGFRs) and fibroblast growth factor receptors (FGFRs), and has been approved for first-line treatment of unresectable hepatocellular carcinoma as monotherapy and first-line treatment of advanced renal cell carcinoma together with pembrolizumab. The potential efficacy of LEN on TNBC patients is also under active investigation[13]. Accumulating data suggest that LEN can inhibit immunosuppressive cells and prevent CD8$^+$ T cell exhaustion *via* blocking VEGFR-mediated and FGFR-mediated pathways while directly killing cancer cells[14,15]. However, LEN surfers from adverse effects associated with non-specific accumulation[16,17], and cannot induce acute local inflammation in the tumor, which is crucial for effective antigen

presentation and activation of antitumor immunity[18]. Vadimezan is an agonist of the stimulator of interferon genes (STING) that is crucial for priming antitumor immunity[19,20]. Activation of STING pathway can elevate the levels of type I interferons[21–23], sufficient intratumoral amount of which has been found a favorable prognostic factor for TNBC patients and has been proved to enhance the efficacy of immunotherapy in multiple murine tumor models including those bearing 4T1 TNBC tumors[24]. However, specific activation of STING pathway in the tumor is required to prevent systemic inflammation.

Given the complementary effects between LEN and vadimezan, we hypothesized that combination treatment of TNBC with the two drugs would be beneficial. A tumor-targeted drug delivery system is crucial to maximize efficacy and minimize side effects[25–27]. Synthetic high-density lipoprotein (sHDL) is a biomimetic and biocompatible nano-carrier that could be functionalized for tumor imaging, vaccination, and treatment[28–30]. The preferential tumor accumulation of the sHDL is associated with its prolonged blood circulation and good tumor penetration[31]. Our previous studies on murine hepatocellular carcinoma model have demonstrated that the intratumoral sHDL showed a high affinity for scavenger receptor class B type 1 (SR-B1), through which the loaded drugs could be directly transported into the cytosol of the cells[32–34]. Since dendritic cells (DCs) also express SR-B1, cytotoxic drug-loaded sHDL would lead to DC malfunction[32]. Given the high expression of SR-B1 on TNBC cells[35] and better cancer cell selectivity of LEN, we envisioned that LEN-loaded sHDL (L-sHDL) should induce potent cancer cell ICD without deteriorating antitumor immunity activation. Herein, we developed a sHDL loaded with both LEN and vadimezan (LV-sHDL) for immunochemotherapy of TNBC (Fig. 1). We hypothesized that the LV-sHDL could recognize the SR-B1 receptors that were highly expressed on 4T1 TNBC cells and deliver LEN and vadimezan directly into the cytosol of the cells for simultaneous activation of ICD and STING pathways. The two drugs were expected to improve antigen presentation and CD8$^+$ T cell activation and relieve the immunosuppression, which would finally induce strong antitumor immunity for tumor control especially when used in combination with ICB.

2. Materials and methods

2.1. Reagents

ApoA-1 peptide (Ac−GFAEKFKEAVKDYFAKFWD−OH, >95%) was purchased from Top Biotechnology Co., Ltd.,
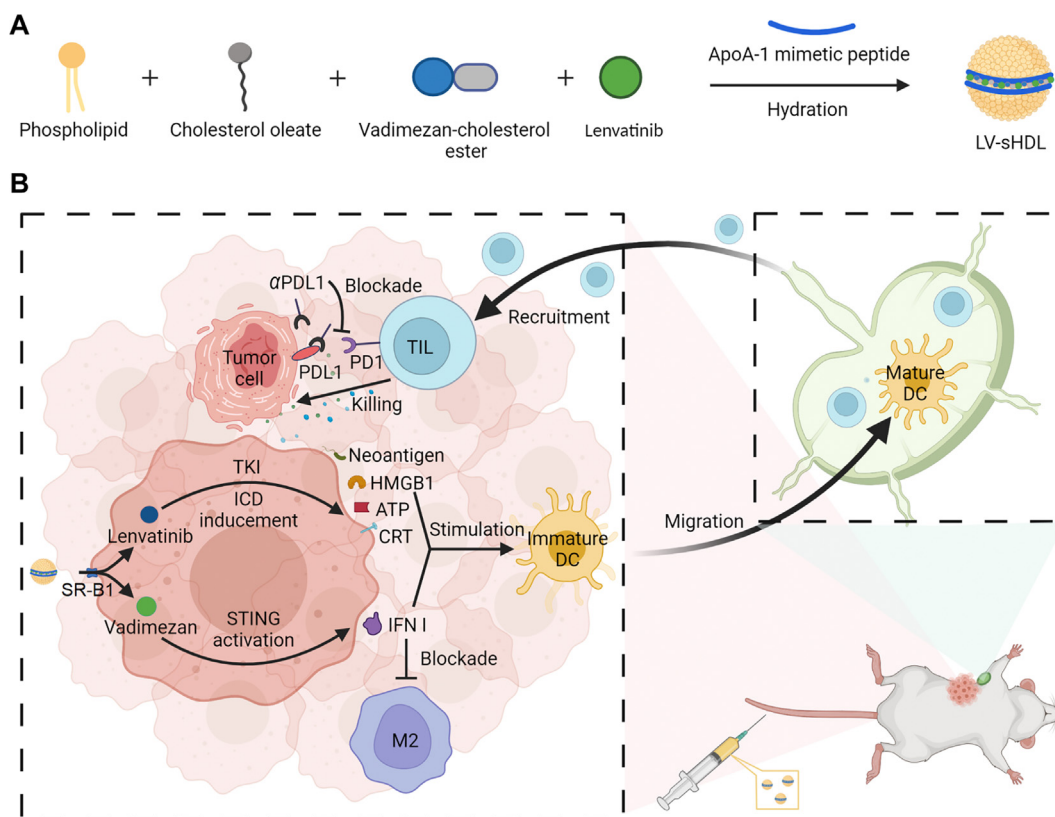
Figure 1 Schematic illustration of the preparation and mechanism of the function of LV-sHDL. (A) Preparation of LV-sHDL. (B) The mechanism of LV-sHDL in tumor tissue. sHDL is applied to deliver LEN and vadimezan together into tumor tissue through a recognition with the SR-B1 on 4T1 tumor cells. LEN is supposed to induce immunogenic cell death (ICD) to trigger antitumor immune response, and vadimezan is expected to activate STING pathway to enhance the dendritic cell (DC) maturation and regulate the immunosuppressive microenvironment simultaneously, thus improving the antitumor effect. Figure was created and reprinted with the permission from with BioRender.com.

(Nanjing, China). Cholesterol oleate (CO), collagenase, hyaluronidase, and DNase were obtained from Sigma–Aldrich (Shanghai, China). Dimyristoylphosphatidylcholine (DMPC) and vadimezan were obtained from Shanghai Coupling Pharmaceutical Technology Co., Ltd., (Shanghai, China). Lenvatinib (LEN) and DiR were obtained from Dalian Meilun Biotechnology Co., Ltd., (Dalian, China). Vadimezan-cholesterol ester (VE) was synthesized and purified according to our previous reports[35,36]. ELISA kits for interferon-γ (IFN-γ), tumor necrosis factor-α (TNF-α), interleukin (IL)-12p40 were obtained from Neobioscience Technology Co., Ltd., (Shenzhen, China). Unless additionally noted, all other reagents were obtained from Sinopharm Chemical Reagent Co., Ltd., (Shanghai, China) and used as received.

2.2. Cells and animals

Murine 4T1 breast cancer cell line was obtained from the cell bank of the Chinese Academy of Sciences and was cultured in RPMI 1640 (Invitrogen, Waltham, MA, USA) supplemented with 10% fetal bovine serum (FBS, Invitrogen) and 1% antibiotics (C100C5, New Cell &Molecular Biotech, Suzhou, China). The cells were maintained at 37 °C in a humidified incubator containing 5% CO_2.

   Female BALB/c mice (18−22 g) and female C57BL/6 mice (18−22 g) were purchased from the Shanghai Experimental

Animal Center (Shanghai, China). OT-I mice (18−22 g) were purchased from Cyagen Biosciences (Shanghai, China). All the animals were maintained in a 12 h/12 h light/dark cycle with free access to food and water. All the animal experiments were approved by the Institutional Animal Care and Use Committee of the Shanghai Institute of Materia Medica, Chinese Academy of Sciences (2021-06-LYP-43).

2.3. Preparation and characterization of sHDLs

All the sHDLs were prepared according to our previous report[32]. Briefly, a thin film of DMPC and CO (25:1, *mol/mol*) was formed under vacuum and re-hydrated with PBS (pH 7.4, containing 0.7 mg/mL ApoA-1 peptide). The suspension was sonicated and centrifuged (7000×*g*, 4 °C, 10 min, H2050R, Xiangyi, Changsha, China), and the supernatant was concentrated using ultrafiltration (COMW = 30 kDa, 7000×*g*, 4 °C, 10 min, H2050R). Fluorescence-labeled sHDLs were prepared as our previous report[32]. LEN-loaded sHDL (L-sHDL), VE-loaded sHDL (V-sHDL), and co-encapsulated sHDL (LV-sHDL, LEN:VE = 1:6, *mol/mol*) were prepared using the same procedure. The amounts of encapsulated drugs of each sHDL were determined by high-performance liquid chromatography (HPLC), and the drug loading (DL) and encapsulation efficiency (EE) were calculated using the following Eqs. (1) and (2) respectively:

$$DL\ (\%) = \frac{W_{\text{drug in sHDL}}}{W_{\text{sHDL}}} \times 100 \tag{1}$$

$$EE\ (\%) = \frac{W_{\text{drug in sHDL}}}{W_{\text{drug added}}} \times 100 \tag{2}$$

The sizes and morphologies of all the sHDLs were examined by bright-field transmission electron microscopy (TEM, Tecnai G2 F20, FEI, Hillsboro, OR, USA) using negative staining methodology, and their ζ-potentials were measured by ZetaSizer (ZS90, Marven Panalytical, Shanghai, China). Potential drug leakage from the sHDLs was determined by examining the drug amount in ultrafiltrate with HPLC. The hemolytic risk of the sHDL was assessed with a previously reported method using 10% Triton X-100 as a positive control[36].

2.4. Biodistribution

To investigate the biodistribution of sHDL and free dyes, 4T1 tumor-bearing mice were established by inoculating 4T1 cells (1×10^6 cells suspended in 100 μL PBS) in the fourth mammary gland (left) of BALB/c mice. When the tumor volume reached ~ 200 mm^3, the mice were randomly assigned to receive either DiR-loaded sHDL or free DiR suspension intravenously (DiR: 4 mg/kg, $n = 3$). The mice were imaged by an IVIS Spectrum imaging system (PerkinElmer, MA, USA) at 1, 2, 4, 6, 12, and 24 h after the injection (Ex/Em = 748/780 nm). The mice were sacrificed by carbon dioxide asphyxiation at the end of the experiment, and the tumors and main organs were collected and imaged.

To quantify the accumulation of LEN in the tumors, 4T1 tumor-bearing mice were dosed with L-sHDL (i.v.) or LEN (i.v. or i.g., 5 mg/kg). The mice were sacrificed at six or 24 h after the administration, and the amounts of LEN in the tumors were determined using HPLC.

2.5. Cellular uptake

To investigate the cellular uptake, 4T1 cells were seeded into a 24-well-plate (8×10^4 cells per well) and cultured for 12 h. The cells were then incubated with Cy5-labelled sHDL for 0.5, 1, 2, and 4 h (Cy5: 20 ng/mL). After being washed with PBS trice, the cells were collected and analyzed on a flow cytometry (FACS Fortessa, BD Biosciences, Franklin Lakes, NJ, USA). All the experiments were performed in triplicate. To examine the subcellular localization, 4T1 cells were seeded on glass slides in a 24-well-plate (4×10^4 cells/well). After a 12 h-incubation, the cells were treated with Cy5-labeled sHDL (Cy5: 10 ng/mL) for 0.5, 1, 2, and 4 h, washed, fixed with 4% paraformaldehyde, permeabilized with 0.1% Triton X-100, stained with Actin-Tracker Green (C2201S, Beyotime, Shanghai, China) and DAPI (422801, Biolegend, San Diego, CA, USA), and imaged on a laser scanning confocal microscopy (TCS-SP8 STED, Leica, Wetzlar, GER) after wash.

2.6. Cytotoxicity assay

4T1 cells were seeded into a 96-well-plate (3×10^3 cells/well) and cultured for 24 h. The medium was replaced with fresh medium containing LEN, L-sHDL, or LV-sHDL of a concentration from 0.1 nmol/L to 100 μmol/L LEN (from 0.6 nmol/L to 600 μmol/L for VE) for 48 h. The viability of cells was measured by CCK-8 Assay according to the manufacturer's protocol (C6005, New Cell &Molecular Biotech).

2.7. Immunogenic cell death in vitro and in vivo

4T1 cells were seeded into a 24-well-plate (4×10^4 cells/well) and cultured for 12 h. The cells were then incubated with PBS, sHDL, LEN, V-sHDL, L-sHDL, or LV-sHDL (LEN: 0.1 μmol/L; VE: 0.6 μmol/L) for 4 h and drug-free medium for 12 h, after which the mediums were collected and centrifuged. The release of ATP and high-mobility group box 1 (HMGB1) were examined by ATP kit (BC0300, Beijing Solarbio Science & Technology Co., Ltd., Beijing, China) and HMGB1 ELISA kit (SEKM-0145, Beijing Solarbio Science & Technology Co., Ltd.) according to the manufacturers' instructions, respectively.

To image the subcellular localization of calreticulin (CRT) and HMGB1, 4T1 cells were seeded onto glass slides in a 24-well-plate (4×10^4 cells/well) 12 h prior to a 4 h incubation with PBS, sHDL, LEN, V-sHDL, L-sHDL, or LV-sHDL (LEN: 0.1 μmol/L; VE: 0.6 μmol/L). The cells were rinsed and further incubated with drug-free medium for 12 h. For CRT imaging, the glass slides were sequentially stained with anti-CRT antibody (DF3139, Affinity Biosciences, Changzhou, China), Alexa Fluor® 488 AffiniPure Rabbit Anti-Mouse IgG (H + L) (33906ES60, Yeasen, Shanghai, China), and DAPI (422801, Biolegend). For HMGB1 imaging, the cells were fixed with 4% paraformaldehyde, permeabilized with 0.1% Triton X-100, and stained with anti-HMGB1 antibody (AF7020, Affinity Biosciences), Alexa Fluor® 647 AffiniPure Rabbit Anti-Mouse IgG (H + L) (33913ES60, Yeasen), and DAPI. The glass slides were washed with PBS thrice after each step and imaged on a laser scanning confocal microscopy.

For ICD determination in vivo, orthotopic 4T1 tumor-bearing mice (tumor volume ~ 100 mm^3) were randomly assigned into one of six groups ($n = 10$) receiving PBS, sHDL, LEN, V-sHDL, L-sHDL, or LV-sHDL (i.v., LEN: 0.5 mg/kg, vadimezan: 2 mg/kg; 1:6 mol/mol, one injection every 4 days for 3 times), respectively. The mice were sacrificed by carbon dioxide asphyxiation, and the tumors were collected 7 days after the last injection, weighed, cut, and digested with a mixture of enzymes (collagenase: 1000 U/mL; hyaluronidase: 1000 U/mL; DNase: 500 U/mL) at 37 °C for 1 h, and filtered through nylon mesh to obtain single-cell suspensions. The cells were counted by a cell counter and then incubated with antibodies against mouse Ep-CAM-PE (118205, Biolegend), Calreticulin (D3E6) XP® Rabbit mAb-Alexa Fluor® 488 (62304S, CST, Danvers, MA, USA) and DAPI ($n = 5$). For the ELISA qualification of HMGB1, tumors were collected, weighed, homogenized in PBS and centrifuged to obtain the supernatant ($n = 5$), according to a previous report[37].

2.8. Dendritic cell maturation in vitro

4T1 cells were seeded into a 24-well-plate (4×10^4 cells/well) and cultured for 12 h. Then, the cells were treated with PBS, sHDL, free LEN, V-sHDL, L-sHDL, LV-sHDL, or LPS (LEN: 0.1 μmol/L; VE: 0.6 μmol/L, LPS: 1 μg/mL) for 4 h before another 24 h co-incubation with bone marrow-derived dendritic cells (BMDCs, 2×10^5 cells/well) that were collected and induced according to our previous report[32]. The mediums were collected and examined for the concentrations of IFN-γ, IL-12p40, and

TNF-α. The cells were collected, stained with antibodies against mouse CD11c-FITC (11-0114-81, eBioscience, San Diego, CA, USA), mouse CD80-PE (12-0801-81, eBioscience), and mouse CD86-APC (105011, Biolegend), and further analyzed by a flow cytometry (BD Biosciences). All the experiments were performed in triplicate.

2.9. Cross priming activity of BMDC in vitro

BMDCs and T cells were prepared according to our previous study[24]. Briefly, B16F10-OVA cells were seeded into 6-well-plates (6×10^5 cells/well) and cultured for 12 h. The cells were treated with PBS, V-sHDL, L-sHDL, and LV-sHDL (LEN: 0.1 μmol/L; VE: 0.6 μmol/L) for 4 h before another 24 h co-incubation with BMDCs (2×10^6 cells/well). CD8$^+$ T cells (from the spleens of OT-I mice) and the pre-cultured BMDCs were purified by CD8a (117304, Biolegend) and CD11c (100704, Biolegend) positive selection through MACS LS column (Miltenyi Biotech, Bergisch Gladbach, GER) with anti-biotin microbeads (130090485, Miltenyi Biotech) following manufacturer's protocol. Purified OT-I CD8$^+$ T cells (2.5×10^5 cells) were labeled with CFSE (21888, Sigma) and then incubated with purified BMDC (5×10^4 cells) for another 48 h. Proliferation of T cells was determined by flow cytometry according to a previous report[38]. All the experiments were performed in triplicate.

2.10. Dendritic cell maturation in vivo

Orthotopic 4T1 tumor-bearing mice were established as described above. Once the tumor volume reached ~ 100 mm^3, mice were randomly divided into six groups ($n = 8$) and injected (i.v.) with PBS, sHDL, LEN, V-sHDL, L-sHDL, or LV-sHDL (LEN: 0.5 mg/kg, vadimezan: 2 mg/kg; 1:6 mol/mol), respectively. The tumor draining lymph nodes (DLNs) were collected three days after the treatment. Single-cell suspensions were prepared from these DLNs ($n = 5$) and stained with corresponding antibodies. The proportion of mature DC (CD80$^+$CD86$^+$) among all DCs was analyzed by a flow cytometry (BD Biosciences), and the cytokine of IFN-γ, IL-12p40, TNF-α of the DLNs homogenate ($n = 3$) were examined by ELISA kits.

2.11. Antitumor immunity

4T1 tumor-bearing mice models were established as described above. When the tumor volume reached ~ 100 mm^3, mice were randomly assigned into six groups ($n = 5$) and injected (i.v.) with PBS, sHDL, LEN, V-sHDL, L-sHDL, or LV-sHDL (LEN: 0.5 mg/kg, vadimezan: 2 mg/kg; 1:6 mol/mol, one injection every 4 days for 3 times), respectively. The tumors were processed as we described above. The cells were counted by a cell counter and then incubated with antibodies against mouse CD45-AlexFlour700 (56-0451-82, eBioscience), mouse CD3-FITC (35-0031-U025, TONBO Biosciences, CA, USA), mouse CD4-PE (12-0041-81, eBioscience), mouse CD8-PE-Cy7 (60-0081-U100, TONBO Biosciences), mouse Foxp3-Percp-Cy5.5 (45-5773-82, eBioscience), mouse IFN-γ-APC (17-7311-81, eBioscience), mouse PDL1-APC (124311, Biolegend) and DAPI (422801, Biolegend). For DC, cells were incubated with antibodies against mouse CD45-AlexFlour700 (56-0451-82, eBioscience), mouse CD11c-FITC (11-0114-81, eBioscience), mouse CD80-PE (12-0801-81, eBioscience), and mouse CD86-APC (105011, Biolegend). For tumor-associated macrophage (TAM), cells were incubated with antibodies against mouse CD45-AlexFlour700 (56-0451-82, eBioscience), mouse CD11b-Percp-Cy5.5 (45-0112-80, eBioscience), mouse F4/80-FITC (11-4801-81, eBioscience), mouse CD206-PE (12-2061-80, eBioscience), and mouse CD86-APC (105011, Biolegend). Cells for Foxp3, IFN-γ, and CD206 analysis were previously fixed and permeabilized by diluted fixation/permeabilization solution (00-5123-43, eBioscience), and then incubated with antibodies against mouse Foxp3, IFN-γ, and CD206 in diluted permeabilization solution (00-8333-56, eBioscience). All the procedures were performed according to the instructions and analyzed by a flow cytometry (BD Biosciences).

2.12. Antitumor efficacy

4T1 tumor models were established as described above. The mice were randomly divided into six groups ($n = 7$) when tumor volumes reached ~ 100 mm^3 and were intravenously injected with PBS, sHDL, LEN, V-sHDL, L-sHDL, or LV-sHDL (LEN: 0.5 mg/kg, vadimezan: 2 mg/kg; 1:6 mol/mol, one injection every 4 days for three injections), respectively. Mice bearing luciferase-expressing 4T1 tumors were used to further assess the anti-metastasis activity of the treatments ($n = 4$). D-Luciferin potassium salt (MB1834-2, Meilun) was injected i.p. 14 days after treatment and images were captured through an IVIS Spectrum imaging system (PerkinElmer, Waltham, MA, USA). Anti-mouse PD-L1 antibody (BE0101, BioXcell, West Lebanon, NH, USA) was injected intraperitoneally at 50 μg per mouse twice (one injection every 7 days). The long (L) and short (W) axis of the tumors, body weight, and survival were monitored every other day. The volume of the tumors was calculated by Eq. (3):

$$\text{Volume} = \left(L \times W^2 \right) / 2 \tag{3}$$

2.13. Statistics

Statistical analysis of data was performed using Prism 6.0 (GraphPad Software). One-way ANOVA was used for comparison of more than two groups, two-way ANOVA with a Bonferroni post-hoc test was used for the tumor growth inhibition data. The Log-Rank test was used for survival rate evaluation. All the tests are two-sided. The difference was considered statistically significant if the P value was less than 0.05. All results were expressed as mean $\pm$ standard deviation (SD).

3. Results

3.1. Preparation and characterization of sHDLs

V-sHDL, L-sHDL, and LV-sHDL were prepared using a film rehydration methodology. Transmission electron microscopy (TEM) images reveal that all these sHDL were comparable in their morphologies and sizes as spherical nanoparticles of 15 nm in diameter (Fig. 2A). Further dynamic light scattering analysis showed that these nanoparticles were all negatively charged with typical ζ-potentials at about -18 mV (Fig. 2B). The typical DL and EE were $2.7 \pm 0.1\%$ and $42.6 \pm 1.0\%$ for LEN and $9.3 \pm 1.2\%$ and $68.4 \pm 1.5\%$ for vadimezan, respectively. The drugs were stably trapped within the nanoparticles with only $\sim 5\%$ leakage after a 24 h-incubation (Fig. 2C). Though an amphiphilic peptide, ApoA-I mimic peptide in sHDL did not cause hemolysis even at 400 μg/mL (Fig. 2D), which was higher
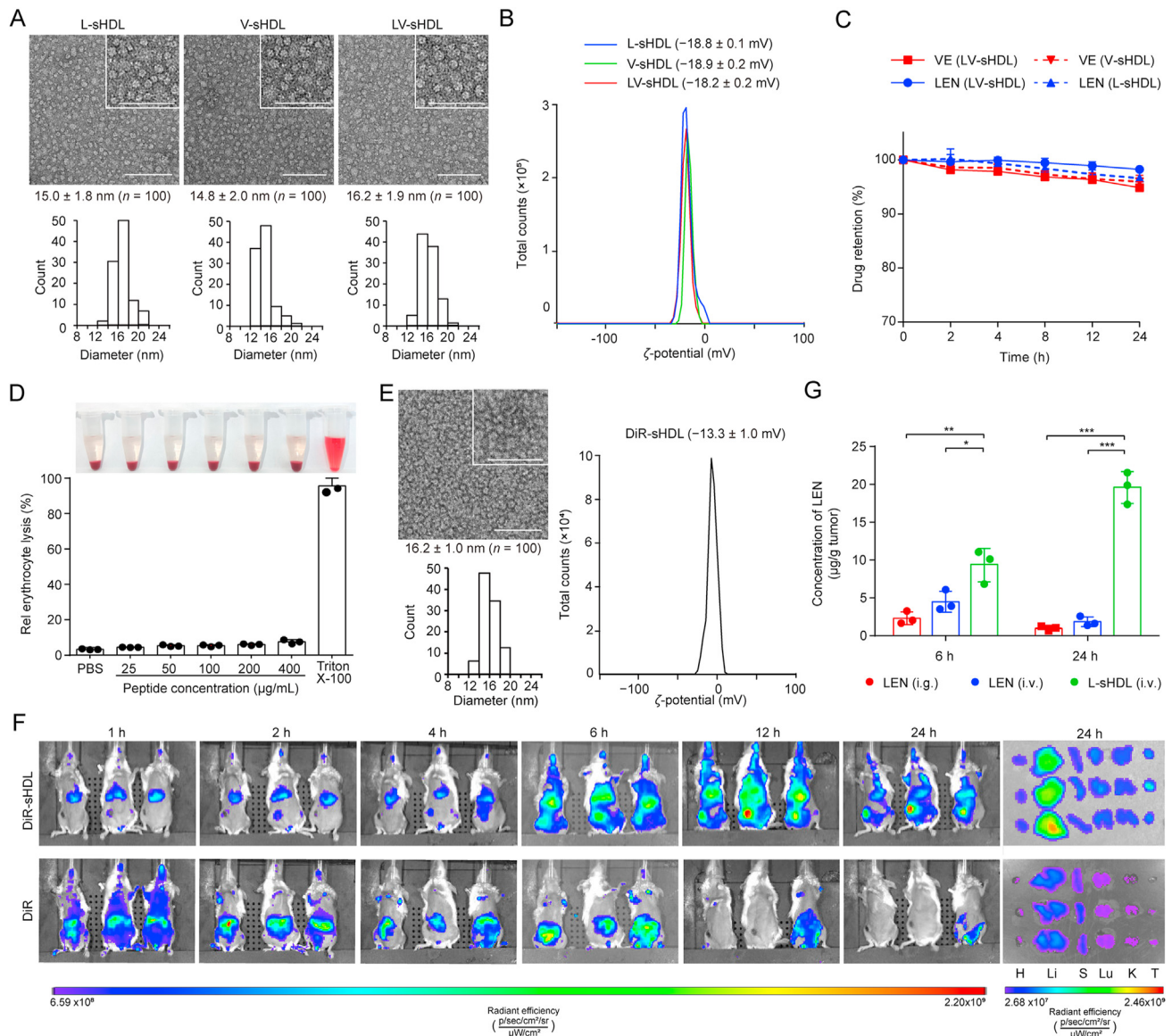
Figure 2 Characterization of sHDLs. TEM images and sizes distribution (A) and ζ-potential (B) of L-sHDL, V-sHDL, and LV-sHDL. Scale bar = 100 nm. (C) Drug release rates of LEN and VE from L-sHDL, V-sHDL, and LV-sHDL within 24 h. (D) Hemolytic risk assessment of sHDL. (E) TEM image, size distribution, and ζ-potential of DiR-sHDL. Scale bar = 100 nm. (F) Near-infrared images of 4T1 tumor-bearing mice captured at different time points and the main organs collected at 24 h after a single injection of DiR-sHDL or DiR. (G) Concentrations of LEN in 4T1 tumors at different time points after one injection of L-sHDL or LEN. Statistical significance was calculated using a two-sided one-way ANOVA test. Data are presented as the mean ± SD (n = 3). *$P < 0.05$, **$P < 0.01$, and ***$P < 0.001$.

than its maximal plasma concentration after intravenous injection. These results reveal that sHDLs could simultaneously adapt two types of drugs without significantly affecting the morphology and size of the sHDLs.

3.2. Tumor accumulation of sHDLs

Given the negligible hemolytic activity of the sHDLs, we explored the tumor accumulation ability of sHDL after intravenous injection in mice bearing orthotopic 4T1 tumors. DiR-loaded sHDL was first prepared and verified to have similar morphology and size as the drug-loaded sHDLs (Fig. 2E). Time-series fluorescence images revealed that sHDL prolonged the retention of DiR in the

animals compared with free DiR, and more DiR was delivered into the tumor and the liver by the sHDL (Fig. 2F). LEN quantification confirmed an ~4-fold increase in liver drug exposure in mice treated with L-sHDL compared with those treated with LEN (Supporting Information Fig. S1), suggesting that attention should be paid to the potential hepatotoxicity of L-sHDL. Further quantification of intratumoral accumulation of LEN in mice treated with L-sHDL (i.v.) or LEN (i.v. or i.g.) (5 mg/kg) further confirmed the tumor-targeted drug delivery capability of sHDL, evidenced by 2.3- and 14.7-fold higher drug deposition at six and 24 h after the treatments, respectively (Fig. 2G). These results demonstrate that sHDL was an efficient carrier for TNBC tumor-targeted drug delivery.

3.3. Cellular uptake and cytotoxicity of sHDL-delivered cargo

The interaction between sHDL and intratumoral cells was mediated by SR-B1 receptor[28,29]. SR-B1 upregulation has been observed in human breast cancer, especially in those with higher aggressiveness such as TNBC[35]. Thus, the expression of SR-B1 by 4T1 cells, AML-12 cells, and BMDC was investigated. Indeed, the Western-blot images show that 4T1 expressed the highest level of SR-B1 among all the cells (Supporting Information Fig. S2). The cellular uptake of sHDL-delivered Cy5 was time-dependent (Fig. 3A), and the dyes were efficiently transported into the cytosol of the cells within 4 h (Fig. 3B). As a result, L-sHDL was more potent (~100-fold decrease in IC_{50}) than free LEN against 4T1 cells (Fig. 3C). On the contrary, L-sHDL and LV-sHDL showed a mild effect on the viability of BMDC at the same range of concentrations (Supporting Information Fig. S3). These results are consistent with our previous reports that sHDL could transport the encapsulated cargo into the cytosol of the cells through SR-B1 receptors.

We then investigated whether LEN could induce ICD and found that LEN triggered leakage of ATP and high mobility group box 1 (HMGB1) from 4T1 cells, which effect was significantly enhanced when the drug was delivered with sHDL (Fig. 3D–E). Confocal images confirmed the leakage of HMGB1 in the cells treated with LEN-containing formulations (Fig. 3F). The same treatments also led to calreticulin (CRT) exposure on the surface of cancer cells. While V-sHDL showed a minor effect on ICD, it elevated pTBK1 and pIRF3 (two major components of the STING pathway[39,40]) and increased secretion of type I interferons (IFN-α/β) by cancer cells (Fig. 3G and Supporting Information Fig. S4), which were crucial for further recruitment and activation of immune cells[41]. These results suggest that LEN and VE in the sHDL triggered two different immune-stimulating pathways, indicating a potential synergistic effect during LV-sHDL-based cancer immunotherapy.

3.4. DC maturation in vitro

Given that LV-sHDL could efficiently induce ICD and type I interferon production, we then evaluated its capability of promoting BMDC maturation in vitro (Fig. 4A). Flow cytometry analysis showed that LV-sHDL (42.8%) induced BMDC maturation ($CD80^+CD86^+$) to an extent comparable to
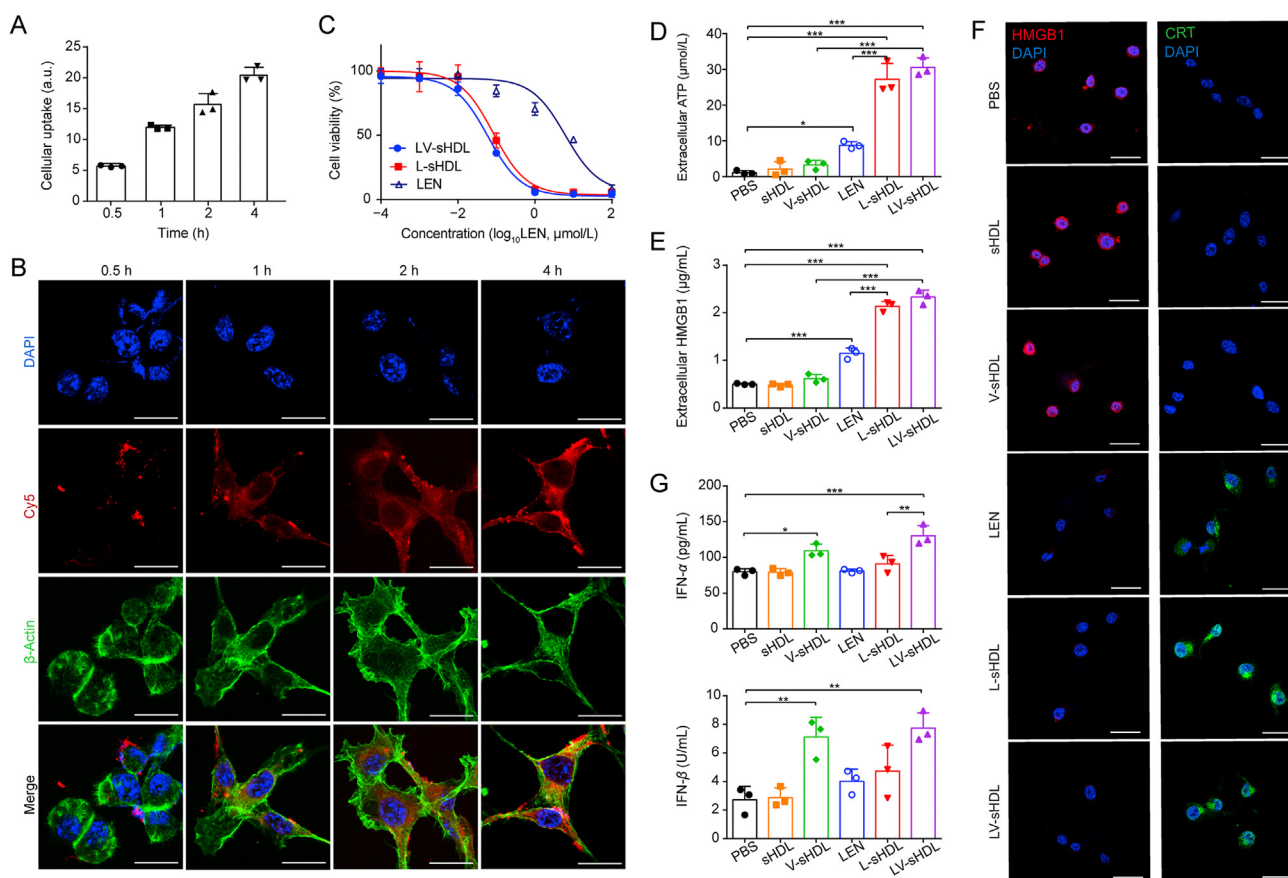

Figure 3 Uptake and efficacy of sHDLs. (A) Flow cytometry analysis of time-dependent cellular uptake of Cy5-labelled sHDL by 4T1 cells. (B) Confocal images of 4T1 cells treated with Cy5-labelled sHDL at different time points. The nucleus and β-actin were stained with DAPI and Actin-Tracker Green, respectively. Scale bar = 20 μm. (C) Cell viability of 4T1 cells after 48 h exposure to LEN, L-sHDL, and LV-sHDL of various concentrations. Quantification of extracellular ATP (D) and HMGB1 (E) in the medium of 4T1 cells after the treatment of different sHDLs. (F) Confocal images of 4T1 cells after 4 h treatment with different sHDLs and another 12 h incubation with medium. The nucleus, HMGB1, and CRT were stained with DAPI, anti-HMGB1 antibody-Alexa Fluor® 647, and anti-CRT antibody-Alexa Fluor® 488, respectively. Scale bar = 20 μm. (G) Quantification of IFN-α and IFN-β secreted by 4T1 cells after the treatment of different sHDLs. Statistical significance was calculated using a two-sided one-way ANOVA test. The data are presented as the mean ± SD ($n = 3$). *$P < 0.05$, **$P < 0.01$, and ***$P < 0.001$.
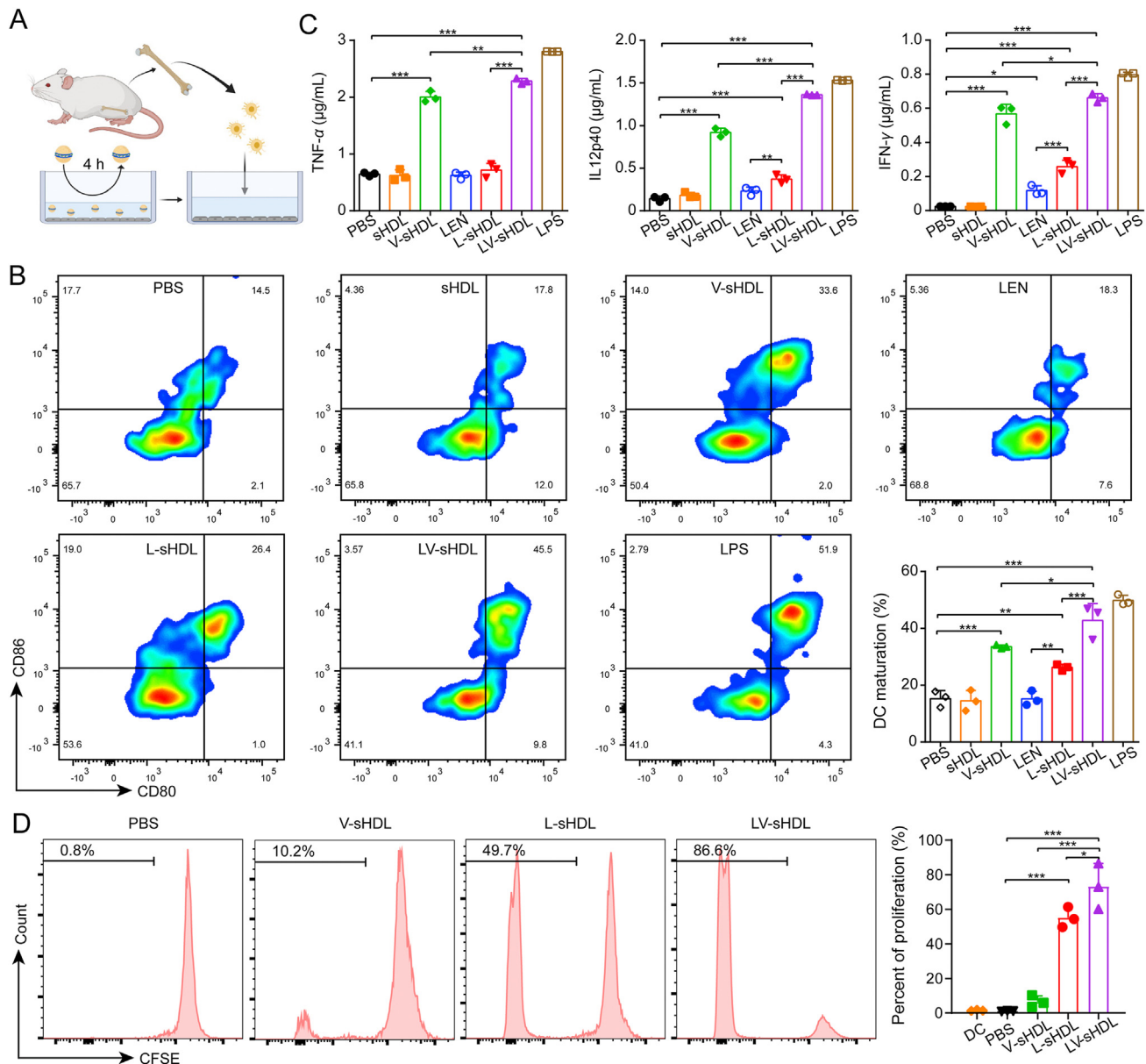
Figure 4 Bone marrow-derived dendritic cells (BMDC) maturation *in vitro*. (A) Schematic illustration of the experimental procedure for in vitro BMDC maturation study. Figure was created and reprinted with the permission from with BioRender.com. (B) Flow cytometry analysis of mature BMDCs (CD80$^+$CD86$^+$) after a 24 h-coculture with sHDL-treated 4T1 cells. BMDCs treated with PBS or LPS were used as negative and positive controls, respectively. (C) Qualification of the secreted TNF-α, IL12p40, IFN-γ in the medium of 4T1 cells after a 24 h-treatment of different sHDLs. (D) Representative histograms plots of CFSE-labelled OT-I cells after 48 h co-incubation with BMDCs. BMDCs were pre-cultured with B16F10-OVA cells pre-treated by different agents for 24 h. Statistical significance was calculated using a two-sided one-way ANOVA test. The data were presented as mean ± SD ($n = 3$). *$P < 0.05$, **$P < 0.01$, and ***$P < 0.001$.

lipopolysaccharide (LPS), and that V-sHDL (33.6%) was slightly less effective followed by L-sHDL (26.3%) mono-therapy (Fig. 4B). On the contrary, sHDL alone was ineffective. The secretion of pro-inflammatory factors including TNF-α, IL12p40, and IFN-γ was also induced by the treatments, and LV-sHDL was more potent than V-sHDL and L-sHDL (Fig. 4C), which agreed with the flow cytometry result. Though L-sHDL triggered much stronger ICD than V-sHDL, the latter was more effective in inducing BMDC maturation than the former. The results indicated that type I interferon pathway

activation played an essential role during DC maturation, which was consistent with our previous reports[24]. To investigate the effect of treatments on DC-mediated T cell proliferation, T cells from OT-I mice were used because of the difficulty to obtain enough antigen-specific T lymphocytes from immunological "cold" TNBC tumors. B16F10-OVA (with comparable SR-B1 expression to 4T1, Supporting Information Fig. S5) and BMDC of the same background were therefore used. Flow cytometry analysis showed that BMDC incubated with L-sHDL-treated B16F10-OVA enhanced T cell proliferation while

V-sHDL showed no significant effect. LV-sHDL again was the most efficient among the tested treatments (Fig. 4D). These results thus support the combination treatment of TNBC with LEN and VE, which killed cancer cells and induced local inflammation, respectively, as both effects were required for effective cancer immun-otherapy.

3.5. Antitumor immunity in vivo

Prompted by the potent activity of LV-sHDL *in vitro*, we then explored the capability of LV-sHDL in priming antitumor immunity *in vivo* on mice bearing orthotopic TNBC tumors. LV-sHDL induced the strongest ICD and STING activation *in vivo* (Fig. 5A–C) and was the most potent in inducing DC maturation (5-fold of PBS group) and local inflammation in the DLNs, followed by V-sHDL and L-sHDL (Fig. 5D–E). LV-sHDL also increased the

intratumoral density of mature DC by 6-fold when compared to PBS (Fig. 5F and Supporting Information Fig. S6). VE-containing sHDLs increased the intratumoral IFN-α/β, while other formulations showed no significant effect (Fig. 5G). Further flow cytometry analysis revealed that LV-sHDL increased intratumoral densities of T lymphocytes (CD3$^+$), cytotoxic T lymphocytes (CD3$^+$CD8$^+$), and active cytotoxic T lymphocytes (CD3$^+$CD8$^+$IFN-γ^+) by 9-, 33-, and 13-fold, respectively, when compared with the PBS group (Fig. 5H–J and Supporting Information Fig. S7). L-sHDL was the second most potent and increased the densities of the above three types of cells by 4-, 10-, and 8-fold, respectively. The data also revealed that the LV-sHDL treatment preferential increased intratumoral CD8$^+$ T cells rather than regulatory T cells (T$_{reg}$, CD3$^+$CD4$^+$Foxp3$^+$), as well as V-sHDL (Fig. 5K and Supporting Information Fig. S8). A similar trend was observed for L-sHDL and LEN but less prominent. VE-
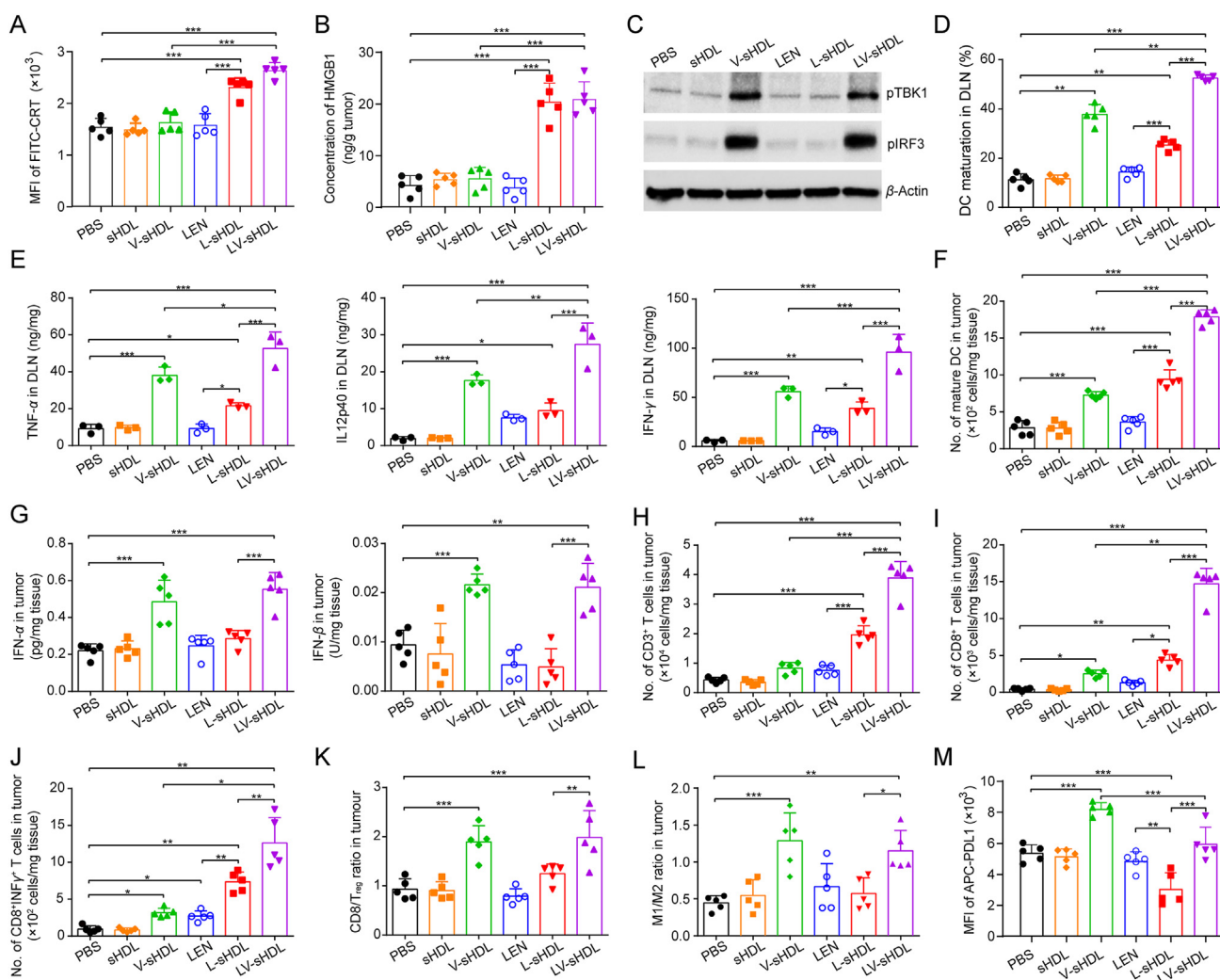

Figure 5 Antitumor immunity induced by the sHDLs *in vivo*. (A) Flow cytometry qualification of CRT levels on tumor cell surface. (B) ELISA qualification of HMGB1 in the tumors. (C) Western-blot analysis of pTBK1 and pIRF3 levels in the tumors. (D) Flow cytometry qualification of the percentage of mature BMDCs (CD80$^+$CD86$^+$) in the DLNs collected 3 days after the administration of different sHDLs ($n = 5$). (E) ELISA qualification of TNF-α, IL12p40, and IFN-γ secretion in the DLNs collected 3 days after the administration of different sHDLs ($n = 3$). In an additional experiment, the tumors were collected 7 days after the last treatment of a three-treatment regimen ($n = 5$). (F) Intratumoral densities of mature DCs. (G) ELISA qualification of IFN-α and IFN-β in the tumors. Intratumoral densities of CD3$^+$ T lymphocytes (H), CD8$^+$ T cells (I), and CD8$^+$IFN-γ^+ T cells (J). (K) CD8$^+$ T cell-to-T$_{reg}$ (CD4$^+$Foxp3$^+$ T cells) ratio. (L) M1-to-M2 ratio. (M) The expression levels of PDL1 on tumor cells after different treatments. Statistical significance was calculated using a two-sided one-way ANOVA test. The data are presented as the mean ± SD. *$P < 0.05$, **$P < 0.01$, and ***$P < 0.001$.

containing sHDLs also increased the ratio of classically activated macrophage (M1) to alternatively activated macrophage (M2) (Fig. 5L, Supporting Information Figs. S9 and S10). Interestingly, V-sHDL increased PDL1 expression on tumor cells while L-sHDL lowered its expression (Fig. 5M), probably because vadimezan stimulated type I interferon-mediated PDL1 expression while LEN inhibited FGFR4-mediated PDL1 expression[14,24]. As a result, the PDL1 expression in LV-sHDL-treated tumors was not altered, indicating that a further combination with the immune checkpoint inhibitor could be beneficial. The results suggested that LEN played a role mainly in increasing the tumor infiltration of immune cells and that VE mainly reversed the immunosuppressive microenvironment by inducing proinflammatory fac-tors[42]. These results collectively confirm that LV-sHDL was the most effective treatment in inducing antitumor immunity.

3.6. Efficacy of LV-sHDL against murine metastatic TNBC

We then evaluated the efficacy of LV-sHDL against metastatic TNBC on mice bearing orthotopic 4T1 tumors (Fig. 6A). After three doses of LV-sHDL, the growth of tumors was retarded by 73.4% compared to that of PBS-treated mice (Fig. 6B). L-sHDL and V-sHDL also slowed tumor growth by 44.7% and 40.8%, respectively. As a result, the median survival time (MST) of the mice extended from 18 days (PBS group) to 28 days after LV-sHDL treatment (Fig. 6C), without significant body weight loss
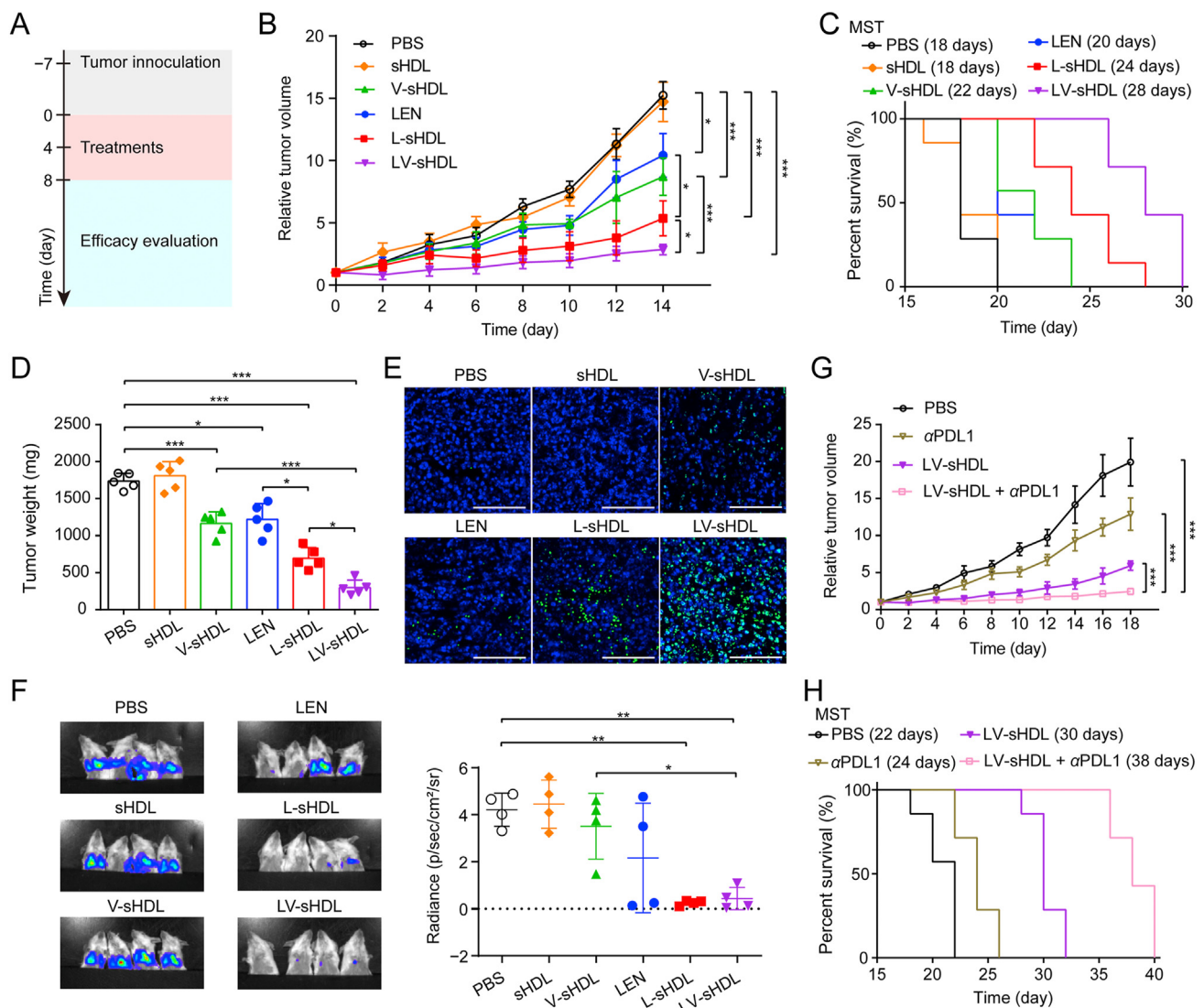

Figure 6 Antitumor activity of sHDLs. (A) Schematic illustration of the treatment strategy. Therapeutic agents were given every four days (i.v., LEN: 0.5 mg/kg, vadimezan: 2 mg/kg; 1:6 *mol/mol*) for 3 times. The relative growth profiles of tumors (B) and survival curves of the mice (C) after different treatments (*n* = 7). The weights of tumors (D), fluorescent images tumor sections after TUNEL staining (E), scale bar = 80 μm, (*n* = 5). (F) Images of the mice bearing luciferase-expressing 4T1 tumors. The pulmonary metastasis was quantified based on the radiance from the lungs (*n* = 4). All the tissues were collected from mice of another experiment 14 days after receiving different treatments. Relative tumor growth profiles (G) and survival curves (H) of mice receiving the indicated treatments on Days 0, 4 and 8 (*n* = 7). Tumor growth inhibition data were analyzed by two-sided two-way ANOVA. The survival data were analyzed by two-sided Log-Rank test. The tumor weight and metastasis data were analyzed using two-sided one-way ANOVA. The data are presented as the mean ± SD. *$P < 0.05$, **$P < 0.01$, and ***$P < 0.001$.

at current dosages (Supporting Information Fig. S11). In consistence, the tumor weights of mice treated with LV-sHDL, L-sHDL, and V-sHDL were 17.1%, 40.0%, and 67.0% of the tumor weight of PBS-treated mice (Fig. 6D). Terminal deoxynucleotidyl transferase-mediated dUTP nick-end labeling (TUNEL) staining also showed that LV-sHDL induced the most extensive cancer cell apoptosis among all the treatments (Fig. 6E). LV-sHDL also inhibited the pulmonary metastasis of 4T1 by >85% (Fig. 6F and Supporting Information Fig. S12). Though sHDL improved drug exposure in the liver, no obvious toxicity was noticed in the major organs even at a higher dosage (6 times of the therapeutic doses, Supporting Information Fig. S13), probably because only a lower dosage was necessary to exert therapeutic effects compared with other formulations[42], indicating a good tolerability of the treatments.

To further improve the therapeutic efficacy, we combined LV-sHDL with an immune checkpoint inhibitor, anti-PDL1 antibody. In contrast with LV-sHDL-treated tumors that showed a fast tumor regrowth at the later phase (after the treatment was stopped), the tumors in mice receiving combination treatments were better controlled (Fig. 6G). The antibody alone only showed mild antitumor activity. Thus, the MST of the mice was further extended to 38 days after the combination therapy (Fig. 6H). Meanwhile, no significant body weight loss was recorded for the combination therapy group (Supporting Information Fig. S14).

4. Discussion

Metastatic TNBC is the most aggressive type of breast cancer with median overall survival of 13−18 months after current treatment options[43]. The efficacy of current combinational immunochemotherapy (nab-paclitaxel plus Atezolizumab) in the clinic relies on the sufficient intratumoral infiltration of CTLs[6,44], and less heavily pretreated metastatic disease is expected to benefit from the treatment[45]. Herein, we developed the LV-sHDL for tumor-targeted and cancer cell-specific delivery of lenvatinib and vadimezan. The LV-sHDL improved intratumoral infiltration and activity of CTLs, and thus inhibited the growth of primary tumors and pulmonary metastasis of 4T1 TNBC model. The efficacy was further improved when LV-sHDL was used in combination with anti-PDL1 antibody.

Combination use of chemotherapy and immunotherapy is crucial to the efficacy of LV-sHDL. Although conventional chemotherapy using cytotoxic agents is routinely adopted in clinic for metastatic TNBC therapy, extensive treatment usually impairs peripheral and local antitumor immunity[46]. Thus, molecularly targeted therapy and immunotherapy combinations are recently being explored in metastatic breast cancer[47]. In our design, LEN, a multitargeted TKI, was used. Despite its potent activity in inducing ICD of cancer cells, LEN was one−two order of magnitude less toxic to BMDC when delivered with sHDL, which is in sharp contrast with chemotherapeutic agent mertansine[32]. In addition, LEN could also inhibit the expression of PDL1 by cancer cells to some extent, which is also beneficial for cancer immunotherapy. Aside from low intratumoral ICD, we previously found that insufficient intratumoral type I interferon was associated with poor response of TNBC tumor to immunotherapy. In our current design, vadimezan, a STING agonist, was co-delivered by sHDL and induced local inflammation that promoted DC maturation and preferential accumulation of M1. The two drugs primed antitumor immunity through two different but cooperative pathways and greatly inhibited the growth of primary tumors and pulmonary metastasis[48]. We used biomimetic sHDL for co-delivery of lenvatinib and vadimezan. The sHDL was previously found to have a long circulation half-life, deep tumor penetration, and SR-B1-mediated specificity[31−33]. Thus, sHDL improved tumor-targeted and 4T1 cell-specific drug delivery, which contributed to the efficacy and safety of the treatment.

Our design successfully increased the intratumoral density of CTLs and their activity. The IFN-γ secreted by active CTLs would however elevate cancer cell expression of PDL1, which could lead to CTL exhaustion. Previous clinical trials revealed that patients with PDL1 positive tumor showed better response to ICB while no difference in survival was observed between patients receiving nab-paclitaxel alone and combination therapy (nab-paclitaxel and ICB)[6,44]. In our case, LEN in LV-sHDL inhibited further upregulation of PDL1 on cancer cells but was not potent enough to downregulate PDL1, indicating persistence of immunosuppression. Increased antitumor activity was indeed achieved when combining LV-sHDL with anti-PDL1 antibody.

5. Conclusions

Insufficient intratumoral accumulation of CTLs and the presence of suppressive tumor microenvironment are two major hurdles that hinder the successful treatment of metastatic TNBC. To overcome these limitations, we have developed an sHDL-based nanoparticle for tumor-targeted and cancer cell-specific co-delivery of lenvatinib and vadimezan, namely LV-sHDL. The two drugs cooperatively induce ICD, promote DC maturation, enhance CTL recruitment, and foster an antitumor microenvironment, which together lead to a successful control of primary tumor growth and pulmonary metastasis. The combination use of LV-sHDL with ICB further improved the efficacy. Given the easy preparation and TNBC-specificity of sHDL, we envision that our LV-sHDL could be a promising treatment for TNBC patients especially those with PDL1-negative tumors.

Author contributions

Chao Zheng and Pengcheng Zhang conceived and designed the project. Chao Zheng and Wen Zhang synthesized and characterized the nanoparticles. Chao Zheng, Wen Zhang, Jinming Wang, Yihui Zhai, Fengqin Xiong, Ying Cai, Xiang Gong and Binyu Zhu performed the experiments. Chao Zheng and Pengcheng Zhang interpreted the data. Chao Zheng, Helen He Zhu, Pengcheng Zhang, Hao Wang and Yaping Li wrote the manuscript. Pengcheng Zhang, Hao Wang and Yaping Li supervised the study.

Conflicts of interest

The authors have no conflicts of interest to declare.

Appendix A. Supporting information

Supporting data to this article can be found online at https://doi.org/10.1016/j.apsb.2022.02.021.

References

1. Waks AG, Winer EP. Breast cancer treatment: a review. *JAMA* 2019;**321**:288−300.
2. Siegel RL, Miller KD, Jemal A. Cancer statistics, 2020. *CA Cancer J Clin* 2020;**70**:7−30.
3. Gradishar WJ, Tjulandin S, Davidson N, Shaw H, Desai N, Bhar P, et al. Phase III trial of nanoparticle albumin-bound paclitaxel compared with polyethylated castor oil-based paclitaxel in women with breast cancer. *J Clin Oncol* 2005;**23**:7794−803.
4. Wei JJ, Long Y, Guo R, Liu XL, Tang X, Rao JD, et al. Multifunctional polymeric micelle-based chemo-immunotherapy with immune checkpoint blockade for efficient treatment of orthotopic and metastatic breast cancer. *Acta Pharm Sin B* 2019;**9**:819−31.
5. Galluzzi L, Buqué A, Kepp O, Zitvogel L, Kroemer G. Immunological effects of conventional chemotherapy and targeted anticancer agents. *Cancer Cell* 2015;**28**:690−714.
6. Schmid P, Adams S, Rugo HS, Schneeweiss A, Barrios CH, Iwata H, et al. Atezolizumab and Nab-paclitaxel in advanced triple-negative breast cancer. *N Engl J Med* 2018;**379**:2108−21.
7. Denkert C, von Minckwitz G, Darb-Esfahani S, Lederer B, Heppner BI, Weber KE, et al. Tumour-infiltrating lymphocytes and prognosis in different subtypes of breast cancer: a pooled analysis of 3771 patients treated with neoadjuvant therapy. *Lancet Oncol* 2018;**19**:40−50.
8. Keenan TE, Tolaney SM. Role of immunotherapy in triple-negative breast cancer. *J Natl Compr Cancer Netw* 2020;**18**:479−89.
9. Bianchini G, Balko JM, Mayer IA, Sanders ME, Gianni L. Triple-negative breast cancer: challenges and opportunities of a heterogeneous disease. *Nat Rev Clin Oncol* 2016;**13**:674−90.
10. Thomas R, Al-Khadairi G, Decock J. Immune checkpoint inhibitors in triple negative breast cancer treatment: promising future prospects. *Front Oncol* 2020;**10**:600573.
11. Karaayvaz M, Cristea S, Gillespie SM, Patel AP, Mylvaganam R, Luo CC, et al. Unravelling subclonal heterogeneity and aggressive disease states in TNBC through single-cell RNA-seq. *Nat Commun* 2018;**9**:3588.
12. Zhou L, Zhang PC, Wang H, Wang DG, Li YP. Smart nanosized drug delivery systems inducing immunogenic cell death for combination with cancer immunotherapy. *Acc Chem Res* 2020;**53**:1761−72.
13. Chung HC, Saada-Bouzid E, Muñoz FL, Yanez E, Im SA, Castanon E, et al. Abstract PS12-07: lenvatinib plus pembrolizumab for previously treated, advanced triple-negative breast cancer: early results from the multicohort phase 2 LEAP-005 study. *Cancer Res* 2021;**81**:PS12. 07.
14. Yi CH, Chen LR, Lin ZF, Liu L, Shao WQ, Zhang R, et al. Lenvatinib targets FGF Receptor 4 to enhance antitumor immune response of anti-programmed cell death-1 in HCC. *Hepatology* 2021;**74**:2544−60.
15. Zhao Y, Zhang YN, Wang KT, Chen L. Lenvatinib for hepatocellular carcinoma: from preclinical mechanisms to anti-cancer therapy. *Biochim Biophys Acta Rev Cancer* 2020;**1874**:188391.
16. Schlumberger M, Tahara M, Wirth LJ, Robinson B, Brose MS, Elisei R, et al. Lenvatinib *versus* placebo in radioiodine-refractory thyroid cancer. *N Engl J Med* 2015;**372**:621−30.
17. Cabanillas ME, Takahashi S. Managing the adverse events associated with lenvatinib therapy in radioiodine-refractory differentiated thyroid cancer. *Semin Oncol* 2019;**46**:57−64.
18. Zhao HK, Wu L, Yan GF, Chen Y, Zhou MY, Wu YZ, et al. Inflammation and tumor progression: signaling pathways and targeted intervention. *Signal Transduct Target Ther* 2021;**6**:263.

19. Ishikawa H, Barber GN. STING is an endoplasmic reticulum adaptor that facilitates innate immune signalling. *Nature* 2008;**455**:674−8.
20. Woo SR, Fuertes MB, Corrales L, Spranger S, Furdyna MJ, Leung MY, et al. STING-dependent cytosolic DNA sensing mediates innate immune recognition of immunogenic tumors. *Immunity* 2014;**41**:830−42.
21. Deng LF, Liang H, Xu M, Yang XM, Burnette B, Arina A, et al. STING-dependent cytosolic DNA sensing promotes radiation-induced type I interferon-dependent antitumor immunity in immunogenic tumors. *Immunity* 2014;**41**:843−52.
22. Schaupp L, Muth S, Rogell L, Kofoed-Branzk M, Melchior F, Lienenklaus S, et al. Microbiota-induced type I interferons instruct a poised basal state of dendritic cells. *Cell* 2020;**181**:1080−96.
23. Ding CY, Song ZL, Shen AC, Chen TT, Zhang A. Small molecules targeting the innate immune cGAS−STING−TBK1 signaling pathway. *Acta Pharm Sin B* 2020;**10**:2272−98.
24. Zhai YH, Wang JM, Lang TQ, Kong Y, Rong R, Cai Y, et al. T lymphocyte membrane-decorated epigenetic nanoinducer of interferons for cancer immunotherapy. *Nat Nanotechnol* 2021;**16**:1271−80.
25. Li QQ, Shi ZQ, Zhang F, Zeng WW, Zhu DW, Mei L. Symphony of nanomaterials and immunotherapy based on the cancer−immunity cycle. *Acta Pharm Sin B* 2021;**12**:107−34.
26. Li J, Burgess DJ. Nanomedicine-based drug delivery towards tumor biological and immunological microenvironment. *Acta Pharm Sin B* 2020;**10**:2110−24.
27. Peng SJ, Xiao FF, Chen MW, Gao HL. Tumor-microenvironment-responsive nanomedicine for enhanced cancer immunotherapy. *Adv Sci* 2022;**9**:e2103836.
28. Kuai R, Li D, Chen YE, Moon JJ, Schwendeman A. High-density lipoproteins: nature's multifunctional nanoparticles. *ACS Nano* 2016;**10**:3015−41.
29. Ng KK, Lovell JF, Zheng G. Lipoprotein-inspired nanoparticles for cancer theranostics. *Acc Chem Res* 2011;**44**:1105−13.
30. Ma XY, Song QX, Gao XL. Reconstituted high-density lipoproteins: novel biomimetic nanocarriers for drug delivery. *Acta Pharm Sin B* 2018;**8**:51−63.
31. Tan T, Hu HY, Wang H, Li J, Wang ZW, Wang J, et al. Bioinspired lipoproteins-mediated photothermia remodels tumor stroma to improve cancer cell accessibility of second nanoparticles. *Nat Commun* 2019;**10**:3322.
32. Wang JY, Meng J, Ran W, Lee RJ, Teng L, Zhang PC, et al. Hepatocellular carcinoma growth retardation and PD-1 blockade therapy potentiation with synthetic high-density lipoprotein. *Nano Lett* 2019;**19**:5266−76.
33. Wang JY, Zheng C, Zhai YH, Cai Y, Lee RJ, Xing JM, et al. High-density lipoprotein modulates tumor-associated macrophage for chemoimmunotherapy of hepatocellular carcinoma. *Nano Today* 2021;**37**:101064.
34. Shen WJ, Azhar S, Kraemer FB. SR-B1: a unique multifunctional receptor for cholesterol influx and efflux. *Annu Rev Physiol* 2018;**80**:95−116.
35. Yuan BY, Wu CS, Wang XW, Wang D, Liu HL, Guo L, et al. High scavenger receptor class B type I expression is related to tumor aggressiveness and poor prognosis in breast cancer. *Tumour Biol* 2016;**37**:3581−8.
36. Ran W, Liu XY, Chang L, Cai Y, Zheng C, Liu J, et al. Self-assembling mertansine prodrug improves tolerability and efficacy of chemotherapy against metastatic triple-negative breast cancer. *J Control Release* 2020;**318**:234−45.
37. Deng HZ, Yang WJ, Zhou ZJ, Tian R, Lin LS, Ma Y, et al. Targeted scavenging of extracellular ROS relieves suppressive immunogenic cell death. *Nat Commun* 2020;**11**:4951.
38. Lu CZ, Guan JH, Lu S, Jin Q, Rousseau B, Lu TS, et al. DNA sensing in mismatch repair-deficient tumor cells is essential for anti-tumor immunity. *Cancer Cell* 2021;**39**:96−108.

39. Chin EN, Yu C, Vartabedian VF, Jia YKM, Gamo AM, Vernier W, et al. Antitumor activity of a systemic STING-activating non-nucleotide cGAMP mimetic. *Science* 2020;**369**:993−9.

40. Burdette DL, Vance RE. STING and the innate immune response to nucleic acids in the cytosol. *Nat Immunol* 2013;**14**:19−26.

41. Zitvogel L, Galluzzi L, Kepp O, Smyth MJ, Kroemer G. Type I interferons in anticancer immunity. *Nat Rev Immunol* 2015;**15**:405−14.

42. Wang R, Yamada T, Arai S, Fukuda K, Taniguchi H, Tanimoto A, et al. Distribution and activity of lenvatinib in brain tumor models of human anaplastic thyroid cancer cells in severe combined immune deficient mice. *Mol Cancer Therapeut* 2019;**18**:947−56.

43. Garrido-Castro AC, Lin NU, Polyak K. Insights into molecular classifications of triple-negative breast cancer: improving patient selection for treatment. *Cancer Discov* 2019;**9**:176−98.

44. Emens LA, Molinero L, Loi S, Rugo HS, Schneeweiss A, Diéras V, et al. Atezolizumab and Nab-paclitaxel in advanced triple-negative breast cancer: biomarker evaluation of the impassion 130 study. *J Natl Cancer Inst* 2021;**113**:1005−16.

45. Kwa MJ, Adams S. Checkpoint inhibitors in triple-negative breast cancer (TNBC): where to go from here. *Cancer* 2018; **124**:2086−103.

46. Axelrod ML, Nixon MJ, Gonzalez-Ericsson PI, Bergman RE, Pilkinton MA, McDonnell WJ, et al. Changes in peripheral and local tumor immunity after neoadjuvant chemotherapy reshape clinical outcomes in patients with breast cancer. *Clin Cancer Res* 2020;**26**: 5668−81.

47. Esteva FJ, Hubbard-Lucey VM, Tang J, L P. Immunotherapy and targeted therapy combinations in metastatic breast cancer. *Lancet Oncol* 2019;**20**:e175−86.

48. Zhang W, Wang F, Hu C, Zhou Y, Gao HL, Hu J. The progress and perspective of nanoparticle-enabled tumor metastasis treatment. *Acta Pharm Sin B* 2020;**10**:2037−53.